

A tunable coupler for suppressing adjacent superconducting qubit coupling

X. Li,^{1,*} T. Cai,^{1,*} H. Yan,¹ Z. Wang,¹ X. Pan,¹ Y. Ma,¹ W. Cai,¹ J. Han,¹ Z. Hua,¹ X. Han,¹ Y. Wu,¹ H. Zhang,¹ H. Wang,¹ Yipu Song,^{1,†} Luming Duan,^{1,‡} and Luyan Sun^{1,§}

¹Center for Quantum Information, Institute for Interdisciplinary Information Sciences, Tsinghua University, Beijing 100084, China

Controllable interaction between superconducting qubits is desirable for large-scale quantum computation and simulation. Here, based on a theoretical proposal by Yan *et al.* [Phys. Rev. Appl. **10**, 054061 (2018)] we experimentally demonstrate a simply-designed and flux-controlled tunable coupler with continuous tunability by adjusting the coupler frequency, which can completely turn off adjacent superconducting qubit coupling. Utilizing the tunable interaction between two qubits via the coupler, we implement a controlled-phase (CZ) gate by tuning one qubit frequency into and out of the usual operating point while dynamically keeping the qubit-qubit coupling off. This scheme not only efficiently suppresses the leakage out of the computational subspace, but also allows for the acquired two-qubit phase being geometric at the operating point only where the coupling is on. We achieve an average CZ gate fidelity of 98.3%, which is dominantly limited by qubit decoherence. The demonstrated tunable coupler provides a desirable tool to suppress adjacent qubit coupling and is suitable for large-scale quantum computation and simulation.

As enormous progress has been made towards more complex networks of qubits [1–7], superconducting quantum circuits have become a promising implementation for quantum simulation [8–10] and fault-tolerant quantum computation [11, 12]. Building large circuits requires long coherent times of the qubit, strong inter-qubit interaction for fast and high-fidelity two-qubit gates, and small to zero coupling between qubits when no interaction is needed. For typical planar circuits with transmon or transmon-type qubits connected through fixed capacitors or quantum buses, strong interaction and variable coupling can be achieved by dynamically adjusting the frequencies of the tunable qubits [4, 13–15] or by applying external microwave drives [16, 17]. Parametric modulation of the frequency of the qubit or the bus has also been used to achieve tunable coupling between qubits [18–26]. However, these approaches could not fully suppress the parasitic ZZ-type coupling between the qubits, the frequency shift of one qubit depending on the state of another, due to the crosstalk even when they are far detuned. This unwanted qubit interaction could be a limited source to degrade the single-qubit gate performance and to accumulate the entanglement phase error. In addition, because of the requirement of the qubit frequency tunability or the relatively small qubit-qubit detunings, these approaches also suffer from the frequency crowding problem.

At the cost of additional circuit complexity, a tunable coupler can help mitigate the above problems of unwanted interactions and frequency crowding, while achieving a controllable qubit interaction without introducing other nonidealities that limit the gate performance. A wide variety of tunable couplers have previously been designed and demonstrated experimentally [27–38]. Tunable coupler is thus desirable for scalable architectures for quantum computation and simulation applications.

In this work, following the theoretical proposal in Ref. 39 we experimentally demonstrate a simply-designed tunable coupler sandwiched between two Xmon qubits in a superconducting circuit [11, 40–42]. By adjusting the coupler frequency, the qubit-qubit coupling strength can be tuned

through a combination of different coupling paths such that a continuous tunability from positive to negative values can be realized. A critical point can be reached to completely turn off the adjacent qubit-qubit coupling. Utilizing the tunable interaction between the two qubits via the coupler, we realize the entangling gates of iSWAP and \sqrt{i} SWAP with a fidelity of 96.8% and 95.0%, respectively. In addition, we implement a controlled-phase (CZ) gate by tuning the qubit frequency into or out of the operating point, where the two qubit states $|11\rangle$ and $|20\rangle$ are resonant, while dynamically keeping the qubit-qubit coupling off by simultaneously tuning the coupler frequency. This scheme not only efficiently suppresses the leakage out of the computational subspace, but also allows for a geometric π phase accumulation on $|11\rangle$ state, which is potentially more robust. We achieve an average CZ gate fidelity of 98.3%. All these gates are dominantly limited by qubit decoherence. The demonstrated tunable coupler provides a simple way to suppress adjacent qubit coupling without degrading the qubit coherence and can be easily applied to large-scale quantum computation and simulation.

Our experimental device consists of three flux-tunable Xmon qubits (Q_1, C, Q_2) [15, 43, 44] with the middle one C serving as the tunable coupler (henceforth referred as the “coupler”), as shown in Fig. 1(a). Figure 1(b) is the schematic of the device. The maximum frequencies of the two qubits and the coupler are $\omega_1^{\max}/2\pi = 4.961$ GHz, $\omega_2^{\max}/2\pi = 4.926$ GHz, and $\omega_c^{\max}/2\pi = 5.977$ GHz. Details of the experimental apparatus and device parameters are presented in the Supplementary Material [45]. We first briefly discuss the operating principle of the tunable coupler following Ref. [39]. The system can be described by the Hamiltonian:

$$H/\hbar = \sum_{i=1,2} \frac{1}{2} \omega_i \sigma_i^z + \frac{1}{2} \omega_c \sigma_c^z + \sum_{i=1,2} g_i (\sigma_i^+ \sigma_c^- + \sigma_c^+ \sigma_i^-) + g_{12} (\sigma_1^+ \sigma_2^- + \sigma_2^+ \sigma_1^-), \quad (1)$$

where ω_α ($\alpha = 1, 2, c$) are the frequencies of Q_1 , Q_2 , and the coupler respectively, $\sigma_\alpha^{z,\pm}$ are the corresponding Pauli Z , raising and lowering operators, g_i ($i = 1, 2$) is the coupling

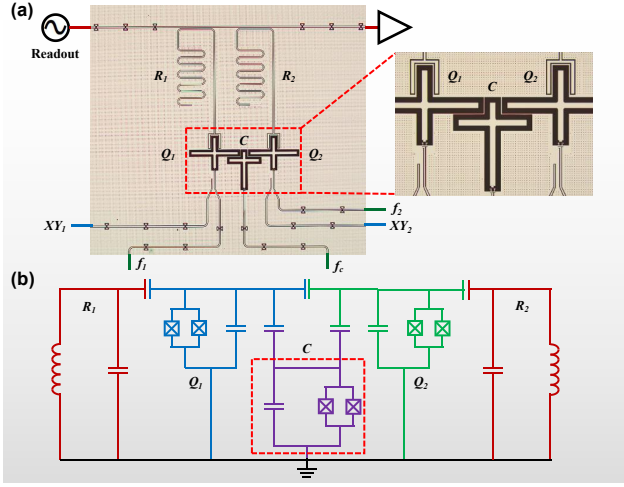


FIG. 1: (a) Optical micrograph of three Xmon qubits with the middle one C serving as a tunable coupler for the two computational qubits (Q_1 and Q_2). Each computational qubit has independent XY and Z control, and is coupled to a separate $\lambda/4$ resonator for simultaneously and individual readout. The coupler also has an individual flux-bias line for a frequency tunability. The combination of direct capacitive coupling and indirect and tunable coupling via the coupler constitutes the total coupling between the two computational qubits. (b) Schematic electrical circuit of the device.

strength between each qubit and the coupler, g_{12} is the direct capacitive coupling strength between the two qubits.

In the strong dispersive regime ($g_i \ll |\Delta_i|$, where $\Delta_i = \omega_i - \omega_c$) and assuming that the coupler mode remains in its ground state, an effective two-qubit Hamiltonian with the variable coupler decoupled can be derived by making the unitary transformation $U = \exp\{\sum_{i=1,2} g_i/\Delta_i(\sigma_i^+ \sigma_c^- - \sigma_i^- \sigma_c^+)\}$ [46, 47] and keeping to second order in g_i/Δ_i :

$$UHU^\dagger/\hbar = \sum_{i=1,2} \frac{1}{2} \tilde{\omega}_i \sigma_i^z + \tilde{g}(\sigma_1^+ \sigma_2^- + \sigma_1^- \sigma_2^+), \quad (2)$$

where $\tilde{\omega}_i = \omega_i + g_i^2/\Delta_i$ is the dressed frequency and

$$\tilde{g} = g_{12} + (g_1 g_2)/\Delta \quad (3)$$

is the effective coupling strength with $1/\Delta = (1/\Delta_1 + 1/\Delta_2)/2$. The interaction between the two qubits thus consists of the direct capacitive coupling and the indirect virtual exchange coupling via the coupler. If $\Delta_i < 0$ (the coupler's frequency is above both qubits' frequencies), the virtual exchange interaction term $(g_1 g_2)/\Delta < 0$. Therefore, the effective coupling \tilde{g} can be tuned from negative to positive monotonically with increasing the coupler frequency. Since this coupling tunability is continuous, a critical value ω_c^{off} can always be reached to turn off the qubit-qubit coupling $\tilde{g}(\omega_c^{\text{off}}) = 0$. Consequently, when the two qubits are detuned, the ZZ -type coupling ξ_{ZZ} is also off.

We now demonstrate the tunability of the qubit-qubit coupling strength \tilde{g} controlled by the coupler's frequency. The experimental pulse sequence is illustrated in Fig. 2(a). Coherent excitation oscillation between Q_1 and Q_2 as a function of

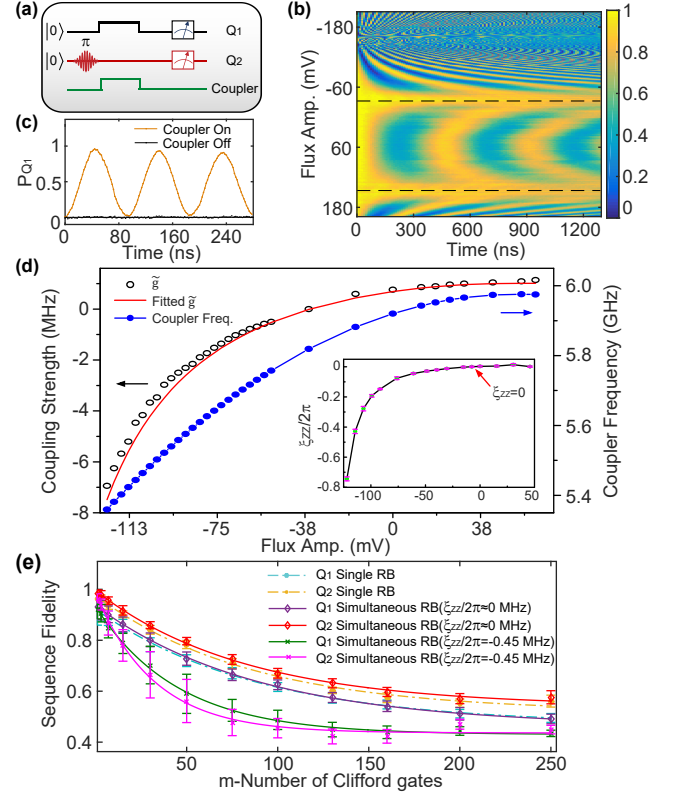


FIG. 2: (a) Pulse sequence to characterize the tunability of the coupler. The two qubits are initialized in the ground state at their sweet spots with a detuning of 35 MHz. The coupler is originally set at $\omega_c/2\pi = 5.905$ GHz where the coupling between the two qubits is nearly off. A π pulse is first to excite Q_2 , followed by two simultaneous fast flux pulses: f_1 brings Q_1 into resonance with Q_2 ; f_c on the coupler to turn on the coupling. After the two qubits interact and evolve for time t , Q_1 and the coupler are pulsed back to the original points for measurements of qubit populations. (b) Population of Q_2 as a function of the amplitude of f_c and t clearly reveals the tunability of the coupling strength. The two dark dashed lines indicate the situation where the coupling is off. (c) Population of Q_1 as a function of time with the coupling on (orange dots) or off (black dots). (d) The effective qubit-qubit coupling strength $\tilde{g}/2\pi$ (black circles) extracted by fitting the oscillation of the qubit excitation in (a) as a function of the flux bias amplitude on the coupler. The coupler frequency (blue dots) can be measured independently by probing the dispersive shift of the qubit frequency when pulsing the coupler into the excited state. The red line represents the simulated coupling strength. Inset: the ZZ crosstalk interaction $\xi_{ZZ}/2\pi$ measured in a Ramsey-type experiment when the two qubits are detuned and at their sweet spots. The red arrow indicates where the coupling is off. (e) Individual and simultaneous RB for Q_1 and Q_2 with $\xi_{ZZ}/2\pi \approx 0$ and -0.45 MHz, respectively.

the flux amplitude of f_c on the coupler and time t is shown in Fig. 2(b), and clearly reveals the change of the coupling strength depending on the coupler frequency. Remarkably, two flux biases of the coupler, at which the qubit-qubit interaction is completely turned off, are observed and marked by two dark dashed lines.

The extracted \tilde{g} indeed varies continuously from positive

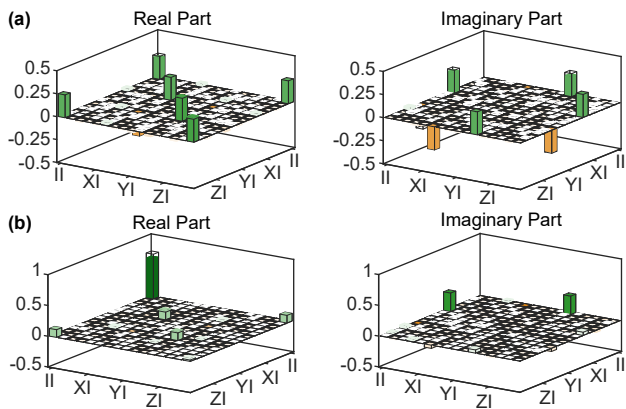


FIG. 3: (a) (b) Bar charts of the measured χ_{exp} from a QPT for iSWAP and \sqrt{i} SWAP with a gate fidelity of 96.8% and 95.0%, respectively. The solid black outlines are for the ideal gate.

to negative values and is in good agreement with theoretical calculations (red curve), as shown in Fig. 2(d). The small discrepancy at large negative coupling regime owes to the deviation of the qubit-coupler coupling from the strong dispersive condition. Given the extracted coupling strength and the frequency detuning of each qubit from the coupler, we can estimate the direct capacitive coupling strength $g_{12} \approx 6.74$ MHz using Eq. (3). We note that a large negative interaction can be reached with the decrease of the coupler frequency approaching the qubit frequency. However, when the coupler frequency is further reduced to be close to the qubit frequency, virtual excitation of the coupler becomes real excitation with an exchange of energy between the qubit and coupler.

We extract ξ_{ZZ} when the two qubits are detuned at their sweet spots using a Ramsey-type experiment (see Supplementary Materials [45]), which involves probing the frequency of Q_1 with Q_2 in either its ground or excited state [48, 49]. The measured ξ_{ZZ} also depends on the coupler frequency and is shown in Fig. 2(d) inset. At the critical coupler frequency $\omega_c^{\text{off}} \approx 5.905$ GHz, indicated by the red arrow, the measured $\xi_{ZZ}/2\pi \approx 1$ kHz and is limited by the current detection scheme. We utilize simultaneous randomized benchmarking (RB) to verify the isolation of two qubits at this configuration. The simultaneous RB gate fidelities of 99.45% and 99.40% are nearly the same as the individual RB gate fidelities of 99.44% and 99.41% for Q_1 and Q_2 respectively, as shown in Fig. 2(e). For comparison, when the two qubits are biased in the same configuration as above but with $\xi_{ZZ}/2\pi = -0.45$ MHz, the simultaneous RB gate fidelities on both qubits are lowered by about 0.54% (Q_1) and 0.93% (Q_2). This contrast illustrates the importance of tunable coupler for precise qubit control.

With the tunability of the coupling, we now move to the implementation of two-qubit entangling gates. The iSWAP and \sqrt{i} SWAP gates are quite natural based on the Hamiltonian of Eq. (2) [34] and their measured χ_{exp} from quantum process tomography (QPT) are presented in Fig. 3 with a gate fidelity of 96.8% and 95.0% respectively. Here we focus on

the controlled-phase (CZ) gate. The CZ gate is implemented by using the usual avoided crossing of the non-computational state $|20\rangle$ with the $|11\rangle$ state [Fig. 4(a)], which is only accessible to $|11\rangle$ and thus provides the conditional nature of the gate to flip the phase if and only if both qubits are excited [14, 50–52].

The full controllable interaction of the coupler allows for turning the coupler ‘on’ or ‘off’ as wish. The ideal scheme of implementing a CZ gate is to have both qubits initialized in the operating point where $|11\rangle$ and $|20\rangle$ have the same energy with the coupling ‘off’, and then slowly turn on the coupler for proper time to implement the gate. This method can avoid adjusting the qubit frequency, and thus reduce the leakage error. However, the unwanted crosstalk of the XY control lines in our device could degrade single-qubit gate performance because of the zero detuning between ω_{12} of Q_1 and ω_{01} of Q_2 . Therefore, the qubits are initially detuned and at their sweet spots with the coupling ‘off’.

The simplest case is to use rectangular fluxes to simultaneously pulse the qubits to the avoided-crossing point and turn on the coupling. Both our measurement and simulation reveal that the leakage out of $|11\rangle$ can be effectively suppressed in the positive coupling regime rather than the negative one. This is evidenced by the observation of high-frequency oscillations [the middle panel in Fig. 4(e)], which cause unwanted leakage error. However, due to the weak positive coupling strength, a relatively long gate time ($t_R = 222$ ns) is required to accomplish the CZ gate. The average CZ gate fidelity is 95.45% from the QPT measurement.

To improve the gate fidelity, we use a different scheme to implement the CZ gate, which can not only efficiently suppress the leakage out of the computational subspace but also allow us to perform the gate in the negative coupling regime with larger interaction strength for a shorter gate time. The experimental flux sequence is shown in Fig. 4(b). We use a gradual flux pulse on Q_2 to tune its frequency to the operating point, while dynamically keeping the coupling ‘off’. This dynamically decoupled regime (DDR) is achieved by applying a flux pulse on the coupler with an appropriate pulse shape calculated by Eq. (3) and is further optimized to assure the zero coupling during the whole qubit frequency changing process (the shaded regions). After that, we slowly turn on the coupling by applying another gradual flux pulse on the coupler and wait for proper time for the two-qubit interaction to acquire the π phase shift on $|11\rangle$. The ‘off’ state of the coupling in the DDR is confirmed by measuring the population change and phase accumulation of $|11\rangle$ state with the same flux pulses as in Fig. 4(b) (the DDR and the dashed line in the middle). The experimental results and sequences are shown in Figs. 4(c) and (d).

We choose an appropriate negative coupling strength to perform the CZ gate, balancing the gate time and qubit-coupler leakage induced by the real excitation of the coupler. The larger interaction strength reduces the CZ gate time to $t_D = 119$ ns [bottom panel in Fig. 4(e)] and the gate fidelity is improved with an average QPT fidelity of 98.3%. The measured

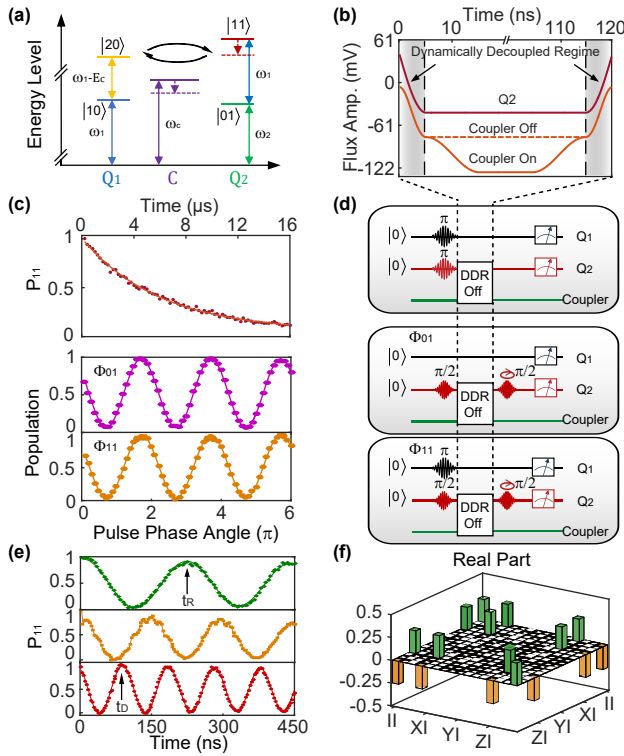


FIG. 4: (a) Schematic to realize the CZ gate using the usual $|11\rangle$ and $|20\rangle$ resonance. (b) Pulse sequence to realize the CZ gate with DDR. The Q_1 frequency is unchanged during the process. A gradual flux pulse (cosine-type for frequency adjustment) on Q_2 is to tune its frequency to the operating point, while a flux pulse on the coupler with an appropriate pulse shape to dynamically keep the coupling ‘off’ (the shaded regions). The coupling is then turned on by applying another gradual flux pulse on the coupler (cosine-type for coupler frequency adjustment) for proper two-qubit interaction time to acquire the required π phase shift on $|11\rangle$. (c) and (d) Confirmation of the ‘off’ state of the coupling in the DDR and the corresponding measurement sequences. Top: The population of $|11\rangle$ state shows purely exponential decay without any oscillation. Middle: phase accumulation of $|01\rangle$ with respect to $|00\rangle$. Bottom: phase accumulation of $|11\rangle$ with respect to $|10\rangle$. The difference between the lower two panels shows zero phase accumulation of $|11\rangle$, confirming zero coupling. (e) Population of $|11\rangle$ in three different schemes to realize the CZ gate. Upper: rectangular pulses to have a positive coupling strength. $t_R = 222$ ns is required for realizing the standard two-qubit CZ gate. Middle: rectangular pulses to have a negative coupling regime. Obvious high-frequency oscillations occur and indicate the leakage out of $|11\rangle$. Lower: DDR pulses to have a large negative coupling but with a smooth oscillation. A CZ gate can be accomplished with a gate time $t_D = 119$ ns. (f) Bar chart of the measured real part of χ_{exp} from a QPT shows a gate fidelity of 98.3%. The solid black outlines are for the ideal gate.

χ_{exp} is shown in Fig. 4(f). Moreover, the observed two-qubit π phase accumulation is geometric, which is potentially noise resilient to frequency fluctuation during the gate operation. The coupler frequency can be further lowered for a higher coupling strength such that the CZ gate time can be reduced to $t_D = 68$ ns. However, due to a larger leakage between the qubit and the coupler, the gate fidelity is slightly lower (see

Supplementary Materials [45]). It is worth mentioning that we also consider a synchronization optimization strategy to mitigate leakages from not only the qubit-qubit $|01\rangle$ and $|10\rangle$ swap channel but also the qubit-coupler real energy exchange channel [53].

In our system, the qubit decoherence error, leakage error, and thermal excitations are the main error sources to limit the gate fidelity. However, the coupler decoherence has little effect on the gate fidelity since it remains in the ground state. Optimization of coupler design for better parameters would be helpful to achieve a higher coupling strength while decreasing the leakage error. Besides, other pulse shapes to turn on the coupling may further suppress the leakage and need future exploration. In addition, improving fabrication technology to minimize crosstalk between XY lines can offer possibility of realizing a more ideal CZ gate [54].

In summary, we experimentally realize a simple prototype of a flux-controlled tunable coupler. The competition between the positive direct and negative indirect coupling allows for a continuous tunability and for switching off the coupling completely. With this coupler, we implement two-qubit entangling iSWAP, $\sqrt{\text{iSWAP}}$, and CZ gates. In particular, the CZ gate is realized with full dynamical control over the qubit-qubit coupling: the coupling is only on at the operating point to acquire a geometric two-qubit phase, while being off during the tuning process of the qubit frequency. We achieve an average CZ gate fidelity of 98.3%, characterized via QPT and dominantly limited by system decoherence. Based on simulation, in the absence of decoherence the CZ gate fidelity could be above 99.99% (see Supplementary Materials [45]). The demonstrated tunable coupler therefore provides a desirable tool to suppress adjacent qubit coupling and is also suitable for large-scale quantum computation and simulation [8–10, 55].

We thank Chengyao Li for the technical support. This work is supported by the State’s Key Project of Research and Development Plan under Grant No. 2016YFA0301902 and 2017YFA0304303, and National Natural Science Foundation of China under Grant No.11874235 and 11674060.

* These two authors contributed equally to this work.

† Electronic address: ypsong@mail.tsinghua.edu.cn

‡ Electronic address: lmduan@tsinghua.edu.cn

§ Electronic address: luyansun@tsinghua.edu.cn

- [1] J. S. Otterbach, R. Manenti, N. Alidoust, A. Bestwick, M. Block, *et al.*, “Unsupervised machine learning on a hybrid quantum computer,” [arXiv:1712.05771](https://arxiv.org/abs/1712.05771) (2017).
- [2] A. Kandala, A. Mezzacapo, K. Temme, M. Takita, M. Brink, J. M. Chow, and J. M. Gambetta, “Hardware-efficient variational quantum eigensolver for small molecules and quantum magnets,” *Nature* **549**, 242 (2017).
- [3] F. Arute, K. Arys, R. Babbush, D. Bacon, and J. C. B. *et al.*, “Quantum supremacy using a programmable superconducting processor,” *Nature* **574**, 505 (2019).

- [4] C. Song, K. Xu, H. Li, Y.-R. Zhang, X. Zhang, W. Liu, Q. Guo, Z. Wang, W. Ren, J. Hao, *et al.*, “Generation of multicomponent atomic schrödinger cat states of up to 20 qubits,” *Science* **365**, 574 (2019).
- [5] Z. Yan, Y. Zhang, M. Gong, and Y. W. *et al.*, “Strongly correlated quantum walks with a 12-qubit superconducting processor,” *Science* **364**, 753 (2019).
- [6] R. Ma, B. Saxberg, C. Owens, N. Leung, Y. Lu, J. Simon, and D. I. Schuster, “A dissipatively stabilized mott insulator of photons,” *Nature* **566**, 51 (2019).
- [7] A. J. Kollár, M. Fitzpatrick, and A. A. Houck, “Hyperbolic lattices in circuit quantum electrodynamics,” *Nature* **571**, 45 (2019).
- [8] I. Buluta and F. Nori, “Quantum simulators,” *Science* **326**, 108 (2009).
- [9] A. A. Houck, H. E. Türeci, and J. Koch, “On-chip quantum simulation with superconducting circuits,” *Nature Physics* **8**, 292 (2012).
- [10] I. M. Georgescu, S. Ashhab, and F. Nori, “Quantum simulation,” *Rev. Mod. Phys.* **86**, 153 (2014).
- [11] M. H. Devoret and R. J. Schoelkopf, “Superconducting circuits for quantum information: an outlook,” *Science* **339**, 1169 (2013).
- [12] E. T. Campbell, B. M. Terhal, and C. Vuillot, “Roads towards fault-tolerant universal quantum computation,” *Nature* **549**, 172 (2017).
- [13] J. Majer, J. M. Chow, J. M. Gambetta, J. Koch, B. R. Johnson, J. A. Schreier, L. Frunzio, D. I. Schuster, A. A. Houck, A. Wallraff, A. Blais, M. H. Devoret, S. M. Girvin, and R. J. Schoelkopf, “Coupling superconducting qubits via a cavity bus,” *Nature* **449**, 443 (2007).
- [14] L. DiCarlo, J. M. Chow, J. M. Gambetta, L. S. Bishop, B. R. Johnson, D. I. Schuster, J. R. Majer, A. Blais, L. Frunzio, S. M. Girvin, and R. J. Schoelkopf, “Demonstration of two-qubit algorithms with a superconducting quantum processor,” *Nature* **460**, 240 (2009).
- [15] J. Kelly, R. Barends, A. G. Fowler, A. Megrant, E. Jeffrey, *et al.*, “State preservation by repetitive error detection in a superconducting quantum circuit,” *Nature* **519**, 66 (2015).
- [16] J. M. Chow, A. D. Córcoles, J. M. Gambetta, C. Rigetti, B. R. Johnson, J. A. Smolin, J. R. Rozen, G. A. Keefe, M. B. Rothwell, M. B. Ketchen, and M. Steffen, “Simple all-microwave entangling gate for fixed-frequency superconducting qubits,” *Phys. Rev. Lett.* **107**, 080502 (2011).
- [17] S. Sheldon, E. Magesan, J. M. Chow, and J. M. Gambetta, “Procedure for systematically tuning up cross-talk in the cross-resonance gate,” *Phys. Rev. A* **93**, 060302 (2016).
- [18] L. Zhou, S. Yang, Y.-x. Liu, C. P. Sun, and F. Nori, “Quantum zero switch for single-photon coherent transport,” *Phys. Rev. A* **80**, 062109 (2009).
- [19] J. D. Strand, M. Ware, F. Beaudoin, T. A. Ohki, B. R. Johnson, A. Blais, and B. L. T. Plourde, “First-order sideband transitions with flux-driven asymmetric transmon qubits,” *Phys. Rev. B* **87**, 220505 (2013).
- [20] Y. X. Liu, C. X. Wang, H. C. Sun, and X. B. Wang, “Coexistence of single- and multi-photon processes due to longitudinal couplings between superconducting flux qubits and external fields,” *New J. Phys.* **16**, 015031 (2014).
- [21] Y. Wu, L. Yang, Y. Zheng, H. Deng, Z. Yan, Y. Zhao, K. Huang, W. J. Munro, K. Nemoto, D. Zheng, C. P. Sun, Y. X. Liu, X. Zhu, and L. Lu, “An efficient and compact quantum switch for quantum circuits,” *npj Quantum Information* **4**, 50 (2018).
- [22] S. A. Caldwell, N. Didier, C. A. Ryan, E. A. Sete, A. Hudson, *et al.*, “Parametrically activated entangling gates using transmon qubits,” *Phys. Rev. Applied* **10**, 034050 (2018).
- [23] M. Reagor, C. B. Osborn, N. Tezak, A. Staley, G. Prawiroatmodjo, *et al.*, “Demonstration of universal parametric entangling gates on a multi-qubit lattice,” *Sci. Adv.* **4**, eaao3603 (2018).
- [24] X. Li, Y. Ma, J. Han, T. Chen, Y. Xu, W. Cai, H. Wang, Y. Song, Z.-Y. Xue, Z.-q. Yin, and L. Sun, “Perfect quantum state transfer in a superconducting qubit chain with parametrically tunable couplings,” *Phys. Rev. Applied* **10**, 054009 (2018).
- [25] W. Cai, J. Han, F. Mei, Y. Xu, Y. Ma, X. Li, H. Wang, Y. P. Song, Z.-Y. Xue, Z.-q. Yin, S. Jia, and L. Sun, “Observation of topological magnon insulator states in a superconducting circuit,” *Phys. Rev. Lett.* **123**, 080501 (2019).
- [26] Y. Xu, Z. Hua, T. Chen, X. Pan, X. Li, J. Han, W. Cai, Y. Ma, H. Wang, Y. Song, Z.-Y. Xue, and L. Sun, “Experimental implementation of universal nonadiabatic geometric quantum gates in a superconducting circuit,” *arXiv:1910.12271* (2019).
- [27] Y.-X. Liu, L. F. Wei, J. S. Tsai, and F. Nori, “Controllable coupling between flux qubits,” *Phys. Rev. Lett.* **96**, 067003 (2006).
- [28] A. Niskanen, K. Harrabi, F. Yoshihara, Y. Nakamura, S. Lloyd, and J. Tsai, “Quantum coherent tunable coupling of superconducting qubits,” *Science* **316**, 723 (2007).
- [29] S. H. W. van der Ploeg, A. Izmailov, A. M. van den Brink, U. Hübner, M. Grajcar, E. Il’ichev, H.-G. Meyer, and A. M. Zagorin, “Controllable coupling of superconducting flux qubits,” *Phys. Rev. Lett.* **98**, 057004 (2007).
- [30] R. Harris, A. J. Berkley, M. W. Johnson, P. Bunyk, S. Govorkov, M. C. Thom, S. Uchaikin, A. B. Wilson, J. Chung, E. Holtham, J. D. Biamonte, A. Y. Smirnov, M. H. S. Amin, and A. Maassen van den Brink, “Sign- and magnitude-tunable coupler for superconducting flux qubits,” *Phys. Rev. Lett.* **98**, 177001 (2007).
- [31] M. S. Allman, F. Altomare, J. D. Whittaker, K. Cicak, D. Li, A. Sirois, J. Strong, J. D. Teufel, and R. W. Simmonds, “rf-squid-mediated coherent tunable coupling between a superconducting phase qubit and a lumped-element resonator,” *Phys. Rev. Lett.* **104**, 177004 (2010).
- [32] R. Bialczak, M. Ansmann, M. Hofheinz, M. Lenander, E. Lucero, M. Neeley, A. O. Connell, D. Sank, H. Wang, M. Weides, *et al.*, “Fast tunable coupler for superconducting qubits,” *Phys. Rev. Lett.* **106**, 060501 (2011).
- [33] Y. Chen, C. Neill, P. Roushan, N. Leung, M. Fang, R. Barends, J. Kelly, B. Campbell, Z. Chen, B. Chiaro, *et al.*, “Qubit architecture with high coherence and fast tunable coupling,” *Physical review letters* **113**, 220502 (2014).
- [34] D. C. McKay, S. Filipp, A. Mezzacapo, E. Magesan, J. M. Chow, and J. M. Gambetta, “Universal gate for fixed-frequency qubits via a tunable bus,” *Physical Review Applied* **6**, 064007 (2016).
- [35] Y. Lu, S. Chakram, N. Leung, N. Earnest, R. K. Naik, Z. Huang, P. Groszkowski, E. Kapit, J. Koch, and D. I. Schuster, “Universal stabilization of a parametrically coupled qubit,” *Phys. Rev. Lett.* **119**, 150502 (2017).
- [36] Q.-M. Chen, Y.-x. Liu, L. Sun, and R.-B. Wu, “Tuning the coupling between superconducting resonators with collective qubits,” *Phys. Rev. A* **98**, 042328 (2018).
- [37] C. Neill, P. Roushan, K. Kechedzhi, S. Boixo, S. Isakov, V. Smelyanskiy, A. Megrant, B. Chiaro, A. Dunsworth, K. Arya, *et al.*, “A blueprint for demonstrating quantum supremacy with superconducting qubits,” *Science* **360**, 195 (2018).
- [38] P. Mundada, G. Zhang, T. Hazard, and A. Houck, “Suppression of qubit crosstalk in a tunable coupling superconducting circuit,” *Phys. Rev. Applied* **12**, 054023 (2019).
- [39] F. Yan, P. Krantz, Y. Sung, M. Kjaergaard, D. L. Campbell, T. P.

- Orlando, S. Gustavsson, and W. D. Oliver, “Tunable coupling scheme for implementing high-fidelity two-qubit gates,” *Physical Review Applied* **10**, 054062 (2018).
- [40] J. Q. You and F. Nori, “Atomic physics and quantum optics using superconducting circuits,” *Nature* **474**, 589 (2011).
- [41] X. Gu, A. F. Kockum, A. Miranowicz, Y. xi Liu, and F. Nori, “Microwave photonics with superconducting quantum circuits,” *Physics Reports* **718-719**, 1 (2017).
- [42] P. Krantz, M. Kjaergaard, F. Yan, T. P. Orlando, S. Gustavsson, and W. D. Oliver, “A quantum engineer’s guide to superconducting qubits,” *Appl. Phys. Rev.* **6**, 021318 (2019).
- [43] R. Barends, J. Kelly, A. Megrant, D. Sank, E. Jeffrey, Y. Chen, Y. Yin, B. Chiaro, J. Mutus, C. Neill, P. O’Malley, P. Roushan, J. Wenner, T. C. White, A. N. Cleland, and J. M. Martinis, “Coherent josephson qubit suitable for scalable quantum integrated circuits,” *Phys. Rev. Lett.* **111**, 080502 (2013).
- [44] R. Barends, J. Kelly, A. Megrant, A. Veitia, D. Sank, E. Jeffrey, T. C. White, J. Mutus, A. G. Fowler, B. Campbell, *et al.*, “Superconducting quantum circuits at the surface code threshold for fault tolerance,” *Nature* **508**, 500 (2014).
- [45] Supplementary Materials .
- [46] A. Blais, J. Gambetta, A. Wallraff, D. I. Schuster, S. M. Girvin, M. H. Devoret, and R. J. Schoelkopf, “Quantum-information processing with circuit quantum electrodynamics,” *Physical Review A* **75**, 032329 (2007).
- [47] S. Bravyi, D. P. DiVincenzo, and D. Loss, “Schrieffer–wolf transformation for quantum many-body systems,” *Annals of physics* **326**, 2793 (2011).
- [48] M. Reed, *Entanglement and quantum error correction with superconducting qubits* (Lulu. com, 2013).
- [49] J. M. Chow, *Quantum information processing with superconducting qubits* (Yale University, 2010).
- [50] F. W. Strauch, P. R. Johnson, A. J. Dragt, C. J. Lobb, J. R. Anderson, and F. C. Wellstood, “Quantum logic gates for coupled superconducting phase qubits,” *Phys. Rev. Lett.* **91**, 167005 (2003).
- [51] M. D. Reed, L. DiCarlo, S. E. Nigg, L. Sun, L. Frunzio, S. M. Girvin, and R. J. Schoelkopf, “Realization of three-qubit quantum error correction with superconducting circuits,” *Nature* **482**, 382 (2012).
- [52] S. Li, A. D. Castellano, S. Wang, Y. Wu, M. Gong, Z. Yan, H. Rong, H. Deng, C. Zha, C. Guo, L. Sun, C. Peng, X. Zhu, and J.-W. Pan, “Realisation of high-fidelity nonadiabatic cz gates with superconducting qubits,” *npj Quantum Information* **5**, 84 (2013).
- [53] R. Barends, C. M. Quintana, A. G. Petukhov, Y. Chen, D. Kafri, *et al.*, “Diabatic gates for frequency-tunable superconducting qubits,” *Phys. Rev. Lett.* **123**, 210501 (2019).
- [54] A. Dunsworth, R. Barends, Y. Chen, Z. Chen, B. Chiaro, A. Fowler, B. Foxen, E. Jeffrey, J. Kelly, P. Klimov, *et al.*, “A method for building low loss multi-layer wiring for superconducting microwave devices,” *Applied Physics Letters* **112**, 063502 (2018).
- [55] O. Kyriienko and A. S. Sørensen, “Floquet quantum simulation with superconducting qubits,” *Phys. Rev. Applied* **9**, 064029 (2018).